Environmental Science and Pollution Research (2023) 30:72966–72977
https://doi.org/10.1007/s11356-023-27586-x

RESEARCH ARTICLE

Adsorption and desorption of polychlorinated biphenyls on biochar colloids with different pyrolysis temperatures: the effect of solution chemistry

Zhongmiao Wang[1] · Kun Yang[1,2] · Daohui Lin[1,2]

Received: 9 February 2023 / Accepted: 8 May 2023 / Published online: 15 May 2023

Abstract

Biochar releases colloidal particles into the environment during applications and aging which can become carriers of pollutants and influence on the environmental risk of pollutants due to the excellent adsorption and migration properties of biochar colloids (BCCs). The adsorption and desorption behaviors of BCCs can be different from their bulk ones due to the colloidal size, which merits specific studies. Herein, the adsorption and desorption of 2,4,4′-trichlorobiphenyl (PCB28) as a representative on BCCs released from bulk biochars prepared from bamboo chips at 300, 500, and 700 C and the effects of solution properties were specifically investigated. Results show that the adsorption was dominated by pore filling and π–π interaction, and thus, BCCs prepared at higher temperature with greater pore volume and aromaticity had higher adsorption of PCB28. Results show that the adsorption was dominated by pore filling and π–π interaction, and thus, BCCs prepared at higher temperature with greater pore volume and aromaticity had higher adsorption of PCB28. The saturation adsorption amounts of PCB28 on BCC300, BCC500, and BCC700 were 21.9, 40.3, and 62.4 mg/g, respectively. It is noteworthy that PCB28 possessed a significant desorption hysteresis from BCCs, with the hysteresis index (Ce = 80 μg/L) increased from 0.380 to 0.661 as the preparation temperature of BCCs rising from 300 to 700 ℃. High concentration of NaCl (100 mmol/L) was unfavorable for the adsorption and desorption. The presence of humic acid or fulvic acid (FA), especially the smaller FA, could inhibit the adsorption and desorption of PCB28 on BCCs due to micropore blocking. In seawater, groundwater, surface water, and soil solution samples, the PCB28 adsorption of BCCs was inhibited to varying degrees in comparison with that in deionized water, and the desorption was noticeably inhibited in the groundwater sample. These findings provide valuable information for the understanding of interactions between BCCs and organic contaminants in natural waters and for the environmental application of biochars as well.

Keywords Biochar · Organic pollutants · Desorption hysteresis · Adsorption · Colloidal behavior

Introduction

Biochar is produced by the pyrolysis of biomass and has received worldwide investigation and applications in improving soil properties, increasing crop yields, combating environmental pollution, and reducing greenhouse gas emissions (Lehmann et al. 2021). Large-scale biochar applications will unavoidably result in the release of nano- and micron-sized biochar colloids (BCCs) into soil and water environments (Aller 2016), and BCCs in soil can be mobilized by surface runoff or groundwater leaching and subsequently migrate to surface water and groundwater environments (Xu et al. 2017; Yang et al. 2019a). BCCs have high mobility and may influence on the spread and biological effectiveness of pollutants as carriers (Ahmad et al. 2014; Kim et al. 2018; Lian and Xing 2017; Yang et al. 2020; Zhang et al. 2010). The adsorption interaction between bulk biochars and organic pollutants has received extensive studies (Lian and Xing 2017; Jellali et al. 2021; Patra et al. 2021). However, the adsorption and desorption behaviors of BCCs that affect the

Responsible Editor: Tito Roberto Cadaval Jr

✉ Daohui Lin
lindaohui@zju.edu.cn

[1] Department of Environmental Science, Zhejiang University, Hangzhou 310058, China

[2] Zhejiang Provincial Key Laboratory of Organic Pollution Process and Control, Zhejiang University, Hangzhou 310058, China

environmental fate and risk of contaminants can be different from their bulk ones due to the colloidal size, which merits to be further studied.

Due to the small particle size and high percentage of O-containing functional groups on surfaces (Yang et al. 2019a), BCCs have very different surface characteristics from their bulk ones in terms of specific surface area, pore volume, aromaticity, and polarity (Yang et al. 2019b), which can impact on the adsorption performance and mechanism for organic pollutants (Hameed et al. 2020; Ma et al. 2019; Wang et al. 2016a, b; Yang et al. 2018a, b, 2020). It has been well reported that properties of both biochar and pollutants can affect the desorption process. Reversible desorption is generally due to reversible adsorption forces between the contaminant and biochar and the open pore structure of the biochar (Ji et al. 2009; Wang et al. 2017a, b; Yang et al. 2018a, b). In contrast, irreversible hysteresis desorption is often due to blockage and rearrangement of the internal void structure of biochar during adsorption (Braida et al. 2003; Jing et al. 2018; Kang et al. 2019), and/or strong adsorption forces between the contaminant and biochar, such as irreversible binding between the contaminant and the functional groups on biochar (e.g., amidation reaction) (Hameed et al. 2020). Current research in general ignores the potential contribution of colloidal properties (aggregation and dispersion) to the adsorption–desorption behavior of organics on BCCs. Agglomeration of carbon nanoparticles, such as carbon nanotubes and fullerene, has been demonstrated to cause hysteresis in the desorption of contaminants (Cheng et al. 2004; Oleszczuk et al. 2009). Likewise, the adsorption–desorption behavior may be affected by the agglomeration and dispersion of BCCs as well.

BCC's adsorption and desorption behavior may vary with the preparation temperature of biochars because of the pyrolysis temperature-dependent properties. Meanwhile, actual environmental conditions are much more complicated than the experimental conditions designed for theoretical studies. The surface characteristics and colloidal behaviors of BCCs are subject to water chemistry, such as pH, ionic strength, and dissolved organic matter (DOM) (Wang et al. 2021). It is reported that the surface electronegativity of BCCs steadily increased as pH rose, changing the surface roughness of BCCs (Yang et al. 2019a); colloidal particles became more electronegative, and their interaction with each other was impacted in the presence of DOM that adsorbed on the surfaces (Dong et al. 2016; Wang et al. 2013); an increase in solution ionic strength reduced the repulsive force between colloidal particles and compressed the thickness of the electric double layer of colloidal particles, enhancing the agglomeration of colloids (Wang et al. 2013; Zhang et al. 2010). Thus, it is likely that the solution chemistry-dependent surface characteristics and colloidal behaviors of BCCs would affect the adsorption–desorption behavior of BCCs to contaminants. Moreover, simulation studies on the effect of a single water quality parameter also need further validation in actual water samples.

Polychlorinated biphenyls (PCBs) are persistent organic pollutants widely present in soil and aquatic environments (Mao et al. 2021; Zhu et al. 2022). Therefore, 2,4,4′-trichlorobiphenyl (PCB28) that has been frequently detected in the environment was chosen as a representative PCBs to investigate the adsorption–desorption behavior of BCCs. The main objectives were to (a) explore the effect of pyrolysis temperature of BCCs on the adsorption–desorption behavior of PCBs, (b) look into the impact of BCCs' agglomeration and dispersion on the adsorption–desorption process in different solution chemistry, and (c) unveil the adsorption–desorption behavior of BCCs in actual water samples. The results will increase our knowledge on the interaction between BCCs and organic contaminants in the environment, and provide theoretical support for the accurate assessment of the environmental risks of biochar in practical applications.

Materials and methods

Materials

PCB28 and PCBs standard solution were obtained from TRE Company (Canada). Hexane (99%, Aladdin, China) for PCB28 extraction was high-performance liquid chromatography (HPLC) grade. NaCl, HCl, NaOH, humic acid (HA), and fulvic acid (FA) for modulating solution chemistry were all of analytical grade and obtained from Sinopharm Chemical Reagent Co., Ltd. (China). Deionized (DI) water (18.2 MΩ cm) was used in all experiments.

Preparation of BCCs

BCCs were extracted from bulk biochars according to Stoke's law. Briefly, bamboo shavings were dried at 65 °C and then carbonized under anoxic conditions in a muffle furnace (Jinan Precision Scientific Instrument Co., Ltd., SX2-12–10, China) at a heating rate of 5 °C min^{-1} until the target pyrolysis temperature reached 300 °C, 500 °C, or 700 °C for 6 h. These obtained bulk biochar particles were designated as BC300, BC500, and BC700, respectively. Bulk biochars were milled by a high-energy planetary ball mill (T-Bota Scitech, QM-3SP2, China) at 40 Hz for 1 h. The resultant biochar powders (1 g) were added into 50 mL of DI water, sonicated (100 W, 45 kHz, Kunshan, KQ-800VDB sonicator, China) for 30 min, and followed by settling for 24 h to extract BCCs (Hameed et al. 2020). The supernatant was filtered through a 0.45-μm cellulose acetate membrane. The solid particles retained on the filter membrane were oven-dried (105 ℃) for 24 h and used as the target BCCs for all

subsequent experiments. The obtained BCCs from BC300, BC500, and BC700 were labeled as BCC300, BCC500, and BCC700, respectively.

Characterization of BCCs

The morphology of BCCs was observed with a scanning electron microscope (Zeiss, Gemini SEM300, Germany). The particle size was calculated by the software (Nano Measurer System, 1.2.5) of SEM image analysis (Chen et al. 2012). The contents of C, H, and N of BCCs were determined using an elemental analyzer (Elementar, varioMICROCHN, Germany). The O content was determined as the weight difference between the raw dried BCCs and the sum of C, H, N, and ash. Nitrogen adsorption–desorption isotherms were measured with a gas sorption analyzer (Quantachrome, Autosorb-1, USA) at 77 K to analyze the specific surface area and pore structure of BCCs. Fourier-transform infrared spectroscopy (FTIR) spectra were obtained using a FTIR spectrometer (Thermo Scientific, Nicolet 6700, USA) in the region of 400–4000 cm^{-1} with a resolution of 4 cm^{-1}. Zeta potentials and hydrodynamic diameters of BCCs (50 mg/L) in different solutions were measured with a Zetasizer (Malvern Instruments, Nano-ZS90, UK).

Adsorption and desorption experiments

The batch adsorption experiments were conducted in polytetrafluoroethylene (PTFE)-lined screw cap glass vials. BCCs after being ultrasonically (100 W, 40 Hz, 25 °C, 10 min) suspended into DI water were used as the stock BCC suspensions (50 mg/L) for the adsorption experiment. The dosages of BCC300, BCC500, and BCC700 for the adsorption experiments were 3, 2, and 0.8 mg/L, respectively. The initial concentrations of PCB28 for the isotherm experiments were within 0–150 μg/L, and 100 μg/L were used for the adsorption kinetics experiments. With these concentration settings, the PCB28 adsorption rate was kept within a measurement–accurate range. The vials were placed on a shaker operated at 150 rpm and 25 ± 1 ℃. The time intervals of the adsorption kinetics experiments were 0, 1, 2, 4, 6, 8, 12, 16, and 24 h. The equilibration time for the isothermal experiment was 24 h which was sufficient to reach the adsorption equilibrium according to the kinetics experiments. Vials were centrifuged at 3500 rpm for 45 min, and the supernatant was put into another clean sample vial with the same volume of hexane solution. PCB28 was extracted from the solution to hexane by vortex at 2000 rpm for 2 min, and the concentration of PCB28 in hexane was determined using gas chromatography (7890B, Agilent, USA) with an HP-5 capillary column (Wu et al. 2022). The temperature of the column was designed to rise from an initial temperature of 120 °C kept for 1 min to 200 °C with a gradient of 35 °C min^{-1} then to 295 °C at a rate of 10 °C $min^{-1}$and held for 0.5 min. The temperatures of the injector port and detector were 260 °C and 300 °C, respectively. The limit of detection was 2 μgL^{-1}, and the recovery was 96.0–102%. PCB28 loss during the adsorption process was excluded by the negligible loss of PCB28 in the vials without addition of BCCs. The adsorption amount of PCB28 on BCCs was calculated by the mass difference of aqueous PCB28 before and after the adsorption.

In the adsorption isotherm experiments, after the adsorption equilibrium and centrifugation, 4 mL of supernatant was quickly replaced by the same volume of background adsorptive solution. The sample vials were sealed and shaken (150 rpm, 25℃) for another 24 h to reach desorption equilibrium. The adsorption amount after the desorption was obtained as above in the adsorption experiment. The desorption rate (*Dr%*) were calculated with Eqs. 1. The sorption–desorption hysteresis in the present study was quantified by the hysteresis index (HI), which has been widely used in past studies to compare the ease of desorption (Huang et al. 1998; Bhandari and Xu 2001; Zhi and Liu 2018).

$$\mathrm{Dr} = \frac{(q_S - q_d) \times 100}{q_S} \tag{1}$$

$$\mathrm{HI} = \frac{q_{ed-}q_{es}}{q_{es}}\Bigg|_{C_e}^{T} \tag{2}$$

where q_s (mg/g) and q_d (mg/g) are the amounts of PCB28 adsorbed on BCCs after the adsorption and desorption processes, respectively; q_{es} (mg/g) and q_{ed} (mg/g) are the adsorption amounts of PCB28 at the adsorption and desorption equilibrium, respectively, and are calculated at the same temperature (T) and equilibrium PCB28 concentration (C_e). q_{es} and q_{ed} at C_e of 10 and 80 μg/L were calculated after the Frendulich model fittings of the adsorption and desorption isotherms, respectively, and the HI values at these two C_e were denoted as HI_1 and HI_2, respectively. The Elovich model, Boyd model, and intraparticle diffusion model were employed to fit the kinetics curves, and Langmuir and Freundlich models were employed to fit the adsorption isotherms. The models are described in Text S1 of the Supporting information (SI)

The effects of solution chemistry on the adsorption and desorption

To investigate the effects of solution chemistry on the adsorption–desorption behavior, the initial concentration of PCB28 was fixed at 100 μg/L, and the dosages of BCC300, BCC500, and BCC700 were 4, 2, and 1 mg/L, respectively. Different concentrations of NaCl (1, 10, and 100 mM) were used to examine the effect of solution ionic strength on the

PCB28 adsorption–desorption of BCCs. To explore the impact of solution pH on the adsorption–desorption, the initial solution pH was adjusted to 5.0, 7.0, and 9.0 with 1 M NaOH and HCl. HA and FA were chosen as DOM representatives to investigate the effect of coexisting DOM on the adsorption–desorption, and their initial concentrations ranged from 0 to 50 mg C/L. The DOM effect curves were plotted with the decrease amounts of adsorption as the vertical coordinate and the logarithmic value of DOM concentration as the horizontal coordinate; the fitted slope (K_{DOM}) indicates the response amplitude of BCCs' adsorption to the variation in DOM concentration.

Seawater, groundwater, surface water, and soil solution were used to investigate the adsorption–desorption behavior of BCCs in natural water environments. The surface water, groundwater, and seawater were sampled from the Yuhangtang River (Hangzhou, China), a local groundwater well (Hangzhou, China), and the South China Sea, respectively. The soil solution was extracted (25 °C, 150 rpm, 3 h) from a local paddy soil with a soil: water mass ratio of 1:9 (Aagot et al. 2001). To effectively remove natural colloids, the collected water samples were filtered with 0.22-μm pore size filter membrane. The pH value, DOM concentration, and anion and cation contents of the water samples were measured using a pH meter (Seven Compact S220, Mettler Toledo, Switzerland), a total organic carbon (TOC) analyzer (TOC-VCPH, Shimadzu, Japan), and an inductively coupled plasma atomic emission spectrometer (7800ICP-MS, Agilent, USA), respectively. The experiments for the water chemistry impacts and natural water samples followed the same procedures for the above adsorption–desorption experiments.

Statistical analysis

All of the adsorption–desorption experiments were performed in triplicate. Statistical analysis was performed using SPSS 23.0. All values were presented as mean ± standard error (SE). Normality and variance homogeneity were verified. Data were subjected to a one-way analysis of variance (ANOVA) followed by Tukey's HSD post hoc test, with $p < 0.05$ taken as a significant difference. BCC properties were used as response variables, and sorption properties were used as explanatory variables for redundancy analysis (RDA) which was carried out with Origin 2022. Correlation analysis between characteristics and sorption properties of BCCs was established by linear regression using SPSS 23.0 and Origin 2022.

Results and discussion

The physicochemical properties of BCCs

The obtained BCCs had slightly different morphologies (Fig. 1a) since the hardness of biochar increased with the increase of pyrolysis temperature (Das et al. 2015), and the particle sizes were mainly within 200–600 nm (Fig. 1b). BCC300 had a substantially larger hydrodynamic size and lower electronegativity than BCC500 and BCC700 in DI

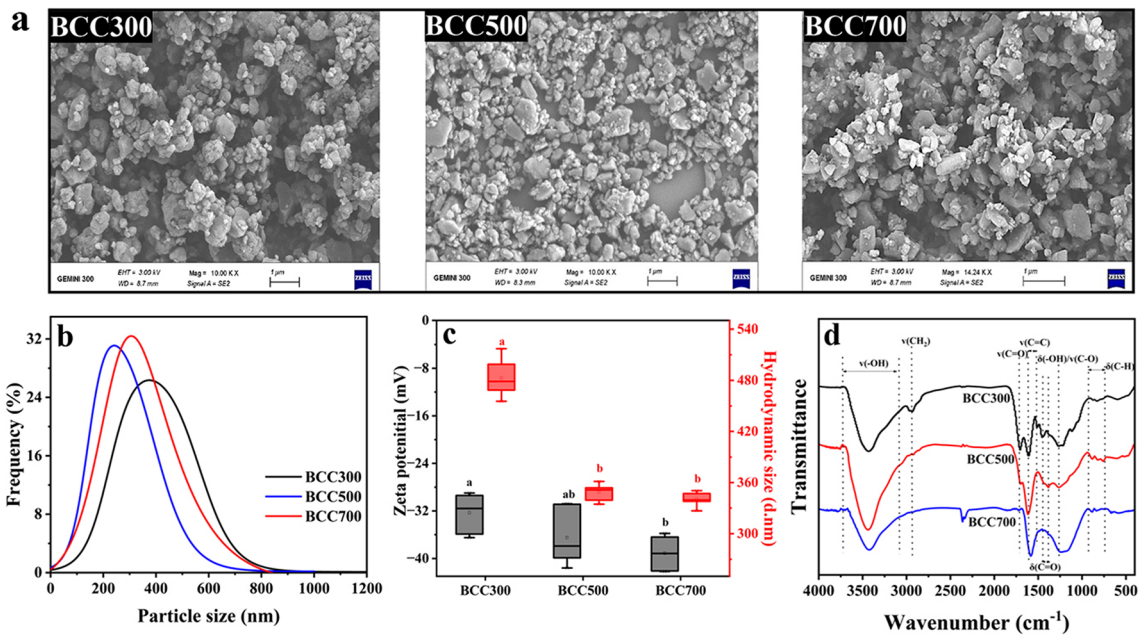

Fig. 1 **a** SEM images, **b** particle size distributions, **c** zeta potential and hydrodynamic size in DI water, and **d** FTIR spectra of BCCs

water (Fig. 1c). With increasing pyrolysis temperature, specific surface area and pore volume of BCCs increased, and the aromaticity also increased as indicated by decreasing H/C elemental ratio, while the polarity decreased as indicated by decreasing O/C and (O + N)/C (Table 1) (Chen et al. 2008; Lin et al. 2007; Yang et al. 2018a, b). The FTIR results (Fig. 1d and Table S1 in SI) further confirmed the increasing aromaticity (C = C bond) and decreasing aliphaticity (alkyl bond) and polarity (O-containing groups) of BCCs with increasing pyrolysis temperature.

Adsorption and desorption of PCB28 on BCCs

Analysis of adsorption kinetics can provide useful information for understanding the mass transfer mechanism of the adsorption process and the rate-limiting steps involved. In accordance with the fitting parameters from the Elovich model (Table S2), the initial adsorption rate (α) had a positive correlation with the change in the pyrolysis temperature of BCCs, while Elovich constant (β) had a negative correlation with the temperature, indicating that BCCs with higher preparation temperatures had more adsorption sites (Chen et al. 2019). The intraparticle diffusion model was further investigated to determine the diffusion mechanism of PCB28 on BCCs and the possible rate-controlling step. As shown in Fig. 2a, the curves of equilibrium adsorption amount (q_e) and $t^{0.5}$ were multilinear, indicating that multiple steps were involved in the adsorption process (Ai et al. 2011; Zhang et al. 2019). During adsorption, PCB28 molecules could be first adsorbed by the outer surfaces of BCCs, and the adsorption rates of BCC500 and BCC700 were 1.76 and 2.67 times higher than that of BCC300 at the initial stage of adsorption (Fig. 2b). Then, PCB28 molecules further entered the interior of micropores and were subsequently adsorbed by the inner surfaces. The Boyd curves (Fig. 2c) were straight lines but did not pass through the origin, indicating that membrane diffusion could be the rate-controlling step in the initial adsorption process of PCB28 on BCCs, after which other mechanisms (intraparticle diffusion) were involved (Ai et al. 2011). BCCs' surface polarity, hydrophobicity, and aromaticity altered as the pyrolysis temperature rose, increasing the BCCs' surface attraction of pollutants (Tong et al. 2019; Wang et al. 2016a, b, 2017a, b) and, as a result, increasing the adsorption rate of BCCs.

Adsorption isotherm fitting can assist understand the mechanism of adsorption and the structural characteristics of the adsorption layer. The isothermal adsorption/desorption curves of BCCs for PCB28 are shown in Fig. 3. Both Langmuir and Freundlich models well fitted the adsorption and desorption isotherms, with the correlation coefficients all higher than 0.95 (Table S3). The Langmuir model fitted adsorption capacity ($Q_{m\text{-}A}$) of BCCs increased with the

Table1 The selected physicochemical properties of BCCs

BCCs	S_{SA} (m^2g^{-1})	V_t (cm^3g^{-1})	V_{mic} (cm^3g^{-1})	D_{aver} (Å)	Elemental composition (%)				Atomic ratio		
					C	H	O	N	H/C	O/C	(O + N)/C
BCC300	20.1	0.067	0.009	19.7	65.8	4.34	29.8	0.225	0.791	0.400	0.342
BCC500	255	0.229	0.127	19.2	77.2	2.93	19.7	0.255	0.455	0.191	0.194
BCC700	336	0.220	0.170	20.5	82.3	1.71	15.9	0.355	0.249	0.143	0.147

S_{SA}, surface area, calculated by multi-point BET method; V_t, total pore volume, calculated at p/p_0 of 0.99; V_{mic}: micropore volume, calculated at p/p^0 of 0.18; D_{aver}, average diameter, calculated by the ratio of quadruple total pore volume to the surface area

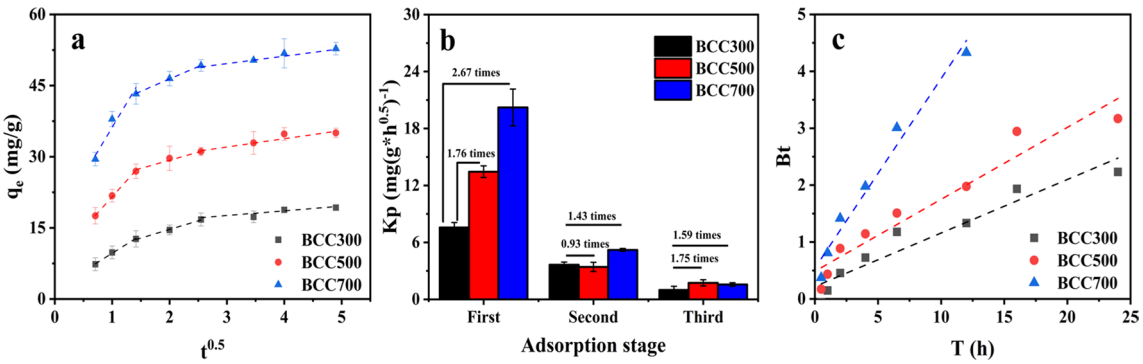

Fig. 2 **a** The adsorption kinetics curves of PCBs on the BCCs fitted by the intraparticle diffusion model. **b** The intraparticle diffusion rates (K_p) of PCBs on BCCs. **c** The Boyd curves of PCBs adsorption kinetics on BCCs

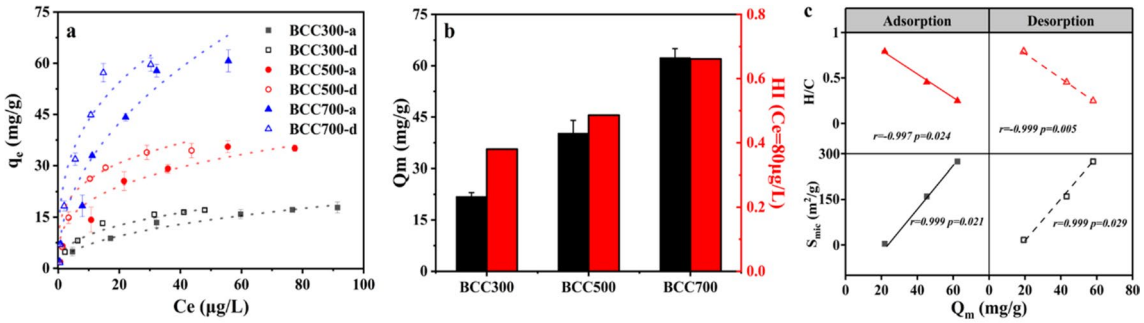

Fig. 3 **a** The adsorption–desorption isotherms of PCB28 on the BCCs. **b** The saturated adsorption capacity (Q_m) and hysteresis index (HI) of BCCs. **c** The relationships between Q_m and physicochemical properties of BCCs. The letters "a" and "d" after BCCs in panel a stand for adsorption and desorption, respectively

pyrolysis temperature, ranging from 21.9 mg/g for BCC300 to 62.4 mg/g for BCC700. BCCs exhibit a significant adsorption effect on PCB28, compared to the adsorption of PCBs by biochar or the adsorption of organic pollutions by nano-biochar/biochar colloids described in the literature (Table S4). Meanwhile, the redundancy analysis results (Fig. S1 in SI) reveal that $Q_{m\text{-}A}$ was not positively linked with micropore specific surface area (S_{ext}) or pore volume (V_{mes}) but was positively correlated with the specific surface area (S_{SA}) and micropore specific surface area (S_{mic}) of BCCs. Figures S2 and 3c further confirm the strong positive correlation between $Q_{m\text{-}A}$ and S_{mic}. The micropore of BCCs was thus presumed as the main adsorption site for PCBs. The geometric radius of PCB28 was 4.277 Å, and the average pore size of BCCs was 19–20 Å (Table 1). Therefore, PCB28 could enter the pore channels of BCCs (Tang et al. 2018), and the pore filling mechanism could control the adsorption of PCB28 by BCCs (Zhou et al. 2022). Figure 3c also shows strong negative correlations of Q_m with H/C; thus, π–π could also contribute to the adsorption of PCB28 by BCCs (Lattao et al. 2014; Xie et al. 2014).

The desorption curves of PCB28 on biochar colloids are presented in Fig. 3a. The adsorption–desorption curves of PCBs on BCCs did not overlap, exhibiting a desorption hysteresis with the desorption hysteresis coefficients at C_e of 10 and 80 μg/L greater than 0. This result suggested that the adsorption of PCB28 by BCCs was irreversible. The order of the hysteresis index HI_2 (C_e = 80 μg/L) was BCC300 (0.380) < BCC500 (0.486) < BCC700 (0.661) (Fig. 3b and Table S5). Thus, PCBs on BCCs with good adsorption performance were more difficult to be desorbed into the environment, and in this regard, BCCs with strong desorption hysteresis may pose relatively less environmental risk. Although the hysteresis index did not correlate well with the physicochemical properties of BCCs as indicated by the p values all high than 0.1 (Fig. S2), the Q_m fitted from the desorption curves also showed significant correlations with the atomic ratios of H/C and S_{mic} (Figs. 3c and S4), suggesting that the desorption process did not affect the adsorption mechanisms of pore filling and π–π interaction between PCBs molecules and BCCs.

The effects of solution pH and ionic strength on the adsorption–desorption behavior

The effects of initial solution pH on the adsorption and desorption of PCBs by BCCs were insignificant, as shown in Fig. 4. Generally, solution pH can affect surface charges of

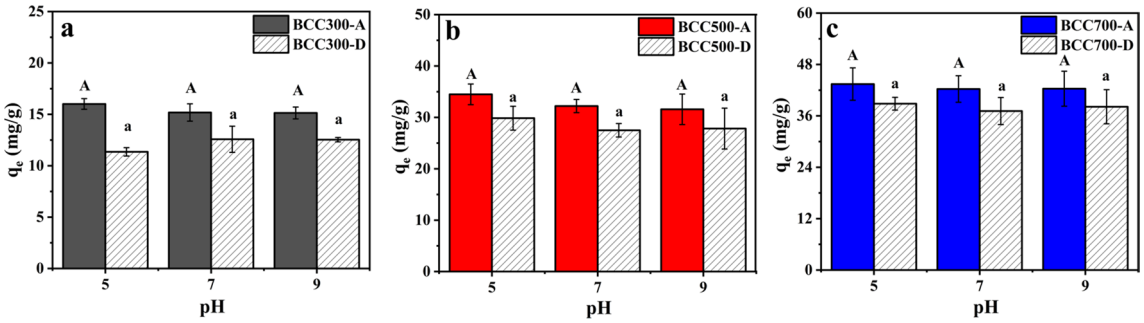

Fig. 4 The effects of solution pH on the adsorption and desorption of PCBs on **a** BCC300, **b** BCC500, and **c** BCC700. The letters "A" and "D" after BCCs in the figure stand for adsorption and desorption, respectively

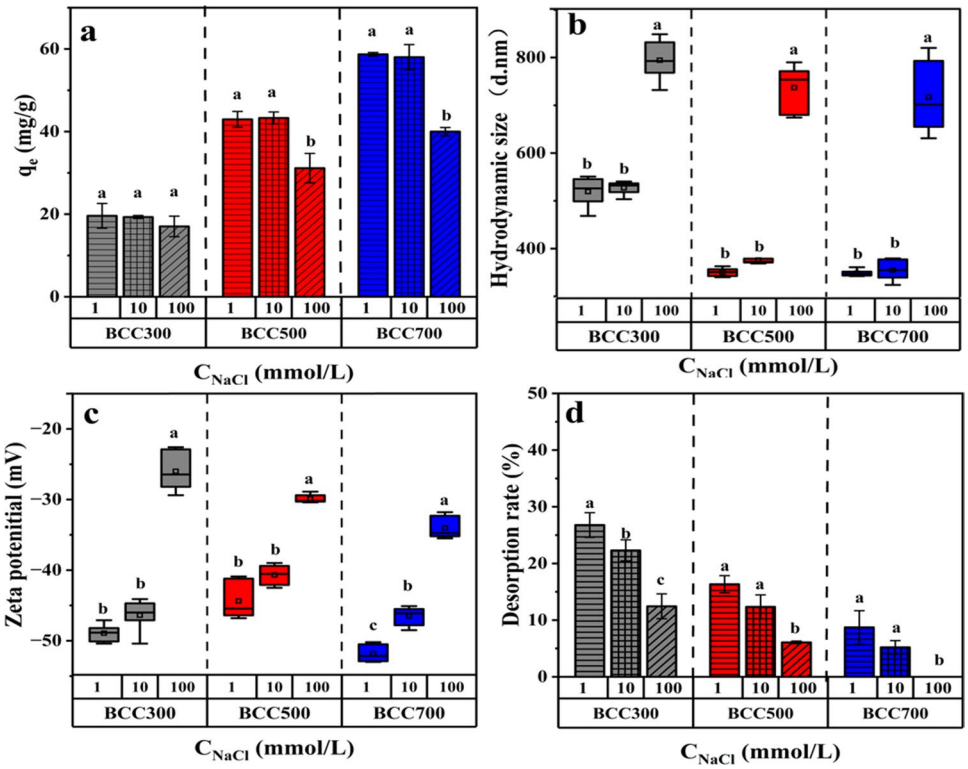

Fig. 5 The effects of ionic concentration on the adsorption–desorption process of PCB28 on BCCs. **a** The adsorption amounts. **b** Hydrodynamic sizes. **c** Zeta potentials. **d** Desorption rates

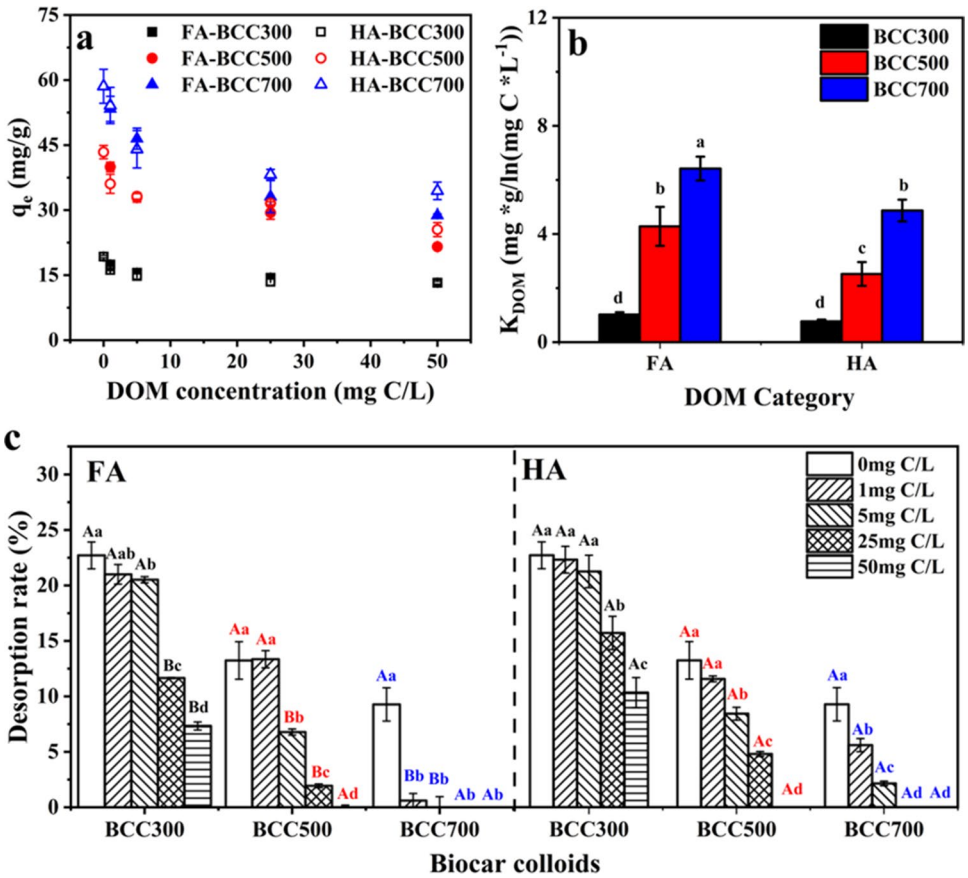

Fig. 6 The effects of DOM type and concentration on the adsorption–desorption process of PCB28 on BCCs. **a** The adsorption amounts, **b** the response amplitude of BCCs' adsorption to the variation in DOM concentration, and **c** the desorption rates. Uppercase letters are labeled to indicate the significant differences in the desorption rate of the same BCCs between HA and FA at the same concentration. Lowercase letters are labeled to distinguish significant differences in the desorption rate of the same BCCs due to changes in the concentration of HA or FA

Table 2 Characteristics of the water samples

Water samples	Cation concentration (mg/L)				Anion concentration (mg/L)			pH	TOC (mg C/L)	IC (mg C/L)
	Na^+	K^+	Ca^{2+}	Mg^{2+}	Cl^-	NO_3^-	SO_4^{2-}			
Sea water	9290 ± 553	300 ± 5	352 ± 12	996 ± 11	13700 ± 91	156 ± 36	954 ± 75	7.42 ± 0.08	3.08 ± 0.35	21.5 ± 0.0
Surface water	11.7 ± 0.3	4.49 ± 0.17	39.1 ± 0.3	6.66 ± 0.12	11.7 ± 0.4	1.08 ± 0	26.1 ± 0.7	7.87 ± 0.00	6.32 ± 0.46	8.28 ± 0.02
Groundwater	35.2 ± 1.4	17.6 ± 0.9	75.9 ± 1.9	6.25 ± 0.28	33.0 ± 0.4	0.41 ± 0	24.9 ± 0.4	7.73 ± 0.03	0.65 ± 0.04	48.4 ± 0.0
Soil solution	3.35 ± 0.12	1.83 ± 0.09	4.78 ± 0.19	0.85 ± 0.04	4.72 ± 0.04	0.21 ± 0	5.41 ± 0.76	6.59 ± 0.19	51.4 ± 1.7	2.53 ± 0.64
DI water	ND	ND	ND	ND	ND	ND	ND	6.90 ± 0.00	0.158 ± 0.062	ND

ND, non-detectable

the adsorbent and/or adsorbate, thereby altering the electrostatic and/or polar (e.g., hydrogen bonding) interactions and the adsorption (Koelmans et al. 2009). However, PCB28 is a non-dissociable compound, and thus, the solution pH change could not affect the adsorption or desorption on BCCs, which also suggests that electrostatic and/or polar (e.g., hydrogen bonding) interactions were not involved in the adsorption–desorption behavior of PCBs on BCCs. The amounts of PCB28 adsorbed on BCCs in solutions with different ionic strength are shown in Fig. 5a. The amounts of PCB28 adsorbed on BCCs kept largely stable in the presence of 1–10 mM NaCl, while the addition of 100 mM NaCl notably decreased the adsorption amounts of PCB28 on BCC300, BCC500, and BCC700 by 13.1%, 27.5%, and 31.9%, respectively. Since PCB28 in solution are in the non-ionic state, the salt effect on electrostatic interaction between PCBs and BCCs could be neglected. With increasing NaCl concentration up to 100 mmol/L, a substantial rise in the hydrodynamic size of BCCs was observed (Fig. 5b), which could be caused by the compression of the electric double layer of BCCs at the high ionic strength (Fig. 5c). The aggregation could inhibit the availability of adsorption sites on BCCs and thus decreased the adsorption of PCBs. The aggregation could also inhibit the desorption process, as indicated by the significantly lower desorption rate of PCBs on BCCs with 100 mmol/L NaCl (Fig. 5d). BCCs were more evenly dispersed in the solution with lower salinity, and under this condition the adsorbed PCBs could be more exposed to solution, facilitating the desorption. In addition, the agglomeration at high ionic concentration could block some micropores of BCCs, inhibiting the desorption of PCBs that previously adsorbed in the micropores (Oleszczuk et al. 2009). The effect of solution salinity on the aggregation of BCCs was apparently positively-correlated with the preparation temperature of BCCs (Fig. 5b), which could explain the apparently greater variation of PCBs adsorption and desorption on BCCs with higher preparation temperature under the effect of solution salinity (Fig. 5a and d).

Influence of DOM on the adsorption–desorption behavior

The impacts of HA and FA on the adsorption and desorption of PCBs on BCCs are depicted in Fig. 6. The adsorption amount of BCCs decreased with increasing DOM concentration. In comparison to the control group without DOM, the inhibition rates of the adsorption amounts of BCC300, BCC500, and BCC700 by 50 mg C/L FA were 31.2%, 50.3%, and 50.8%, respectively, and were 30.1%, 41.1%, and 41.2% by the same concentration of HA, respectively (Fig. 6a). The responses of the PCBs adsorption on BCC300 to the concentration variations of FA and HA had no significant difference (Fig. 6b). In contrast, the PCBs adsorptions on BCC500 and BCC700 were more sensitive to the variation of DOM, and

FA had significantly higher effects on the adsorption than HA (Fig. 6b). DOM can occupy adsorption sites or block the path of adsorbates to reach adsorption sites, leading to a decrease in adsorption (Chowdhury et al. 2013; Koelmans et al. 2009; Zhou et al. 2015). The HA colloids had hydrodynamic diameters within 120–350 nm, whereas 11.9% and 25.2% of the FA colloids were smaller than 1 nm and within 3–6 nm, respectively (Fig. S5). Therefore, in comparison with HA, FA could have higher potential moving into the micropores of BCCs and thereby inhibited the accessibility of PCBs to the adsorption sites in the micropores (Hu et al. 2022). Furthermore, FA is more hydrophilic than HA (Islam et al. 2020), and thus, the adsorption of FA on BCCs could have a higher inhibition effect on the PCBs adsorption through the hydrophobic interaction. The desorption of PCBs from BCCs especially those with higher preparation temperatures was hindered by a rise in DOM concentration (Fig. 6c). Pore blockage by DOM could prevent the desorption of organic chemicals from the pore channel of porous materials (Aschermann et al. 2019). BCC500 and BCC700 had more micropores than BCC300 (Table 1), which made the desorption of PCBs from them was more sensitive to the presence of DOM.

Adsorption–desorption characteristics of BCCs in actual water samples

The physicochemical properties of the four water samples are shown in Table 2. The adsorption amount of PCBs on BCC300 remain stable in the water samples and DI water, while more or less decrease in PCBs adsorption on the other two BCCs were observed in the four water samples in comparison with that in DI water (Fig. 7a). The adsorption amounts of PCBs on BCC500 and BCC700 in the groundwater sample were not significantly different from those in DI water. The TOC and ion concentrations of the groundwater were very low and could thus have no significant effect on the adsorption of PCBs. The TOC concentration of the surface water was 6.32 mg C/L, which could cause the decrease in PCBs adsorption on BCC500 and BCC700. The soil solution contained higher TOC content, which could inhibit more PCBs adsorption on BCC500 and BCC700. The adsorption amounts PCBs on BCC500 and BCC700 in the seawater sample were the lowest among the four water samples, which could be caused by the highest salinity that increased the aggregation of BCCs and thus blocked the adsorption sites.

The desorption of PCBs on BCCs in the four water samples is shown in Fig. 7b. The desorption rates of PCBs on the three BCCs in the groundwater all significantly lowered in comparison with that in DI water, whereas the fluctuations of desorption rates in the other three water were samples were insignificant from the DI water group. The desorption results of BCCs in the natural water samples did not match well with the earlier findings of single-factor effects, which might be because several environmental factors simultaneously acted on the desorption process in natural waters. Further research is still needed to determine the exact percentage contribution of each impacting factor.

Conclusions

In this study, BCCs were prepared at 300, 500, and 700℃, and PCB28 was used as a probe to examine the adsorption–desorption behavior of PCBs on the BCCs. The adsorption capacities of BCCs for PCBs were positively related to the micropore area of BCCs, while negatively related to the polarity. Mainly due to the pore filling adsorption mechanism, the desorption hysteresis of PCBs on BCCs became more pronounced with an increase in the preparation temperature of BCCs. High ionic strength could inhibit the adsorption and desorption of PCBs due to the facilitated BCCs aggregation and micropore blockage. For example, the addition of 100 mM NaCl significantly reduced adsorption amounts of PCB28 on BCC300, BCC500, and BCC700 by 13.1%, 27.5%, and 31.9%, respectively, and no detectable desorption of PCB28 from BCC700 was observed. The adsorptions of FA and HA, especially the smaller FA, could also block micropores of BCCs, especially the higher-temperature BCCs that had more micropores, and thus affected the adsorption–desorption behavior of BCCs.

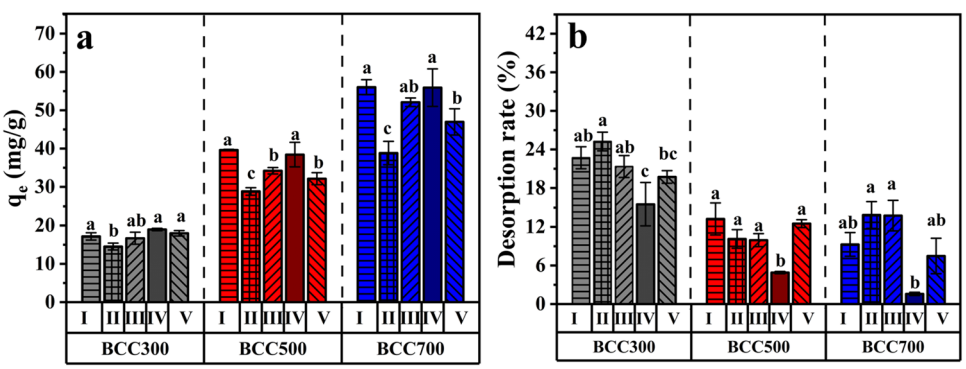

Fig. 7 The adsorption amounts (**a**) and desorption rates (**b**) of PCBs on BCCs in actual water samples. I: DI water; II: sea water; III: surface water; IV: ground water; V: soil solution

In practical applications, the adsorption capacity of biochar colloids could more or less decrease in seawater, surface water, groundwater, and soil solutions, while the exact contributions of complex impact factors in nature waters to the adsorption–desorption behavior of BCC merits more studied. The adsorption by BCCs may increase the environmental risk of hydrophobic pollutants (e.g., PCBs) by facilitating their migration and dispersion, while the desorption hysteresis of hydrophobic pollutants on BCCs (especially high-temperature BCCs) may greatly limit their bioaccessibility. Overall, the interaction between BCCs and pollutants can alter environmental behaviors and ecological effects of BCCs and pollutants, which shall be considered in their environmental risk assessments.

Supplementary Information The online version contains supplementary material available at https://doi.org/10.1007/s11356-023-27586-x.

Author contribution Zhongmiao Wang: conceptualization, methodology, validation, formal analysis, investigation, visualization, writing—original draft, and writing—review and editing. Kun Yang: investigation. Daohui Lin: conceptualization, methodology, validation, writing—review and editing, supervision, and funding acquisition.

Funding This work was supported by the National Natural Science Foundation of China (42192573, U21A20163), National Key Research and Development Program of China (2022YFC3702104), and Zhejiang Provincial Natural Science Foundation of China (LD21B070001).

Data availability The datasets used or analyzed during the current study are available from the corresponding author on reasonable request.

Declarations

Ethics approval This is not applicable.

Consent to participate This is not applicable.

Consent to publish This is not applicable.

Competing interests The authors declare no competing interests.

References

Aagot N, Nybroe O, Nielsen P, Johnsen K (2001) An altered Pseudomonas diversity is recovered from soil by using nutrient-poor Pseudomonas-selective soil extract media. Appl Environ Microbiol 67(11):5233–5239. https://doi.org/10.1128/AEM.67.11.5233-5239.2001

Ahmad M, Rajapaksha AU, Lim JE, Zhang M, Bolan N, Mohan D, Vithanage M, Lee SS, Ok YS (2014) Biochar as a sorbent for contaminant management in soil and water: a review. Chemosphere 99:19–33. https://doi.org/10.1016/j.chemosphere.2013.10.071

Ai LH, Zhang CY, Meng LY (2011) Adsorption of methyl orange from aqueous solution on hydrothermal synthesized Mg-Al layered double hydroxide. J Chem Eng Data 56(11):4217–4225. https://doi.org/10.1021/je200743u

Aller MF (2016) Biochar properties: transport, fate, and impact. Crit Rev Environ Sci Technol 46(14–15):1183–1296. https://doi.org/10.1080/10643389.2016.1212368

Aschermann G, Neubert L, Zietzschmann F, Jekel M (2019) Impact of different DOM size fractions on the desorption of organic micropollutants from activated carbon. Water Res 161:161–170. https://doi.org/10.1016/j.watres.2019.05.039

Bhandari A, Xu FX (2001) Impact of peroxidase addition on the sorption – desorption behavior of phenolic contaminants in surface soils. Environ Sci Technol 35:3163–3168. https://doi.org/10.1021/es002063n

Braida WJ, Pignatello JJ, Lu YF, Ravikovitch PI, Neimark AV, Xing BS (2003) Sorption hysteresis of benzene in charcoal particles. Environ Sci Technol 37(2):409–417. https://doi.org/10.1021/es020660z

Chen BL, Zhou DD, Zhu LZ (2008) Transitional adsorption and partition of nonpolar and polar aromatic contaminants by biochars of pine needles with different pyrolytic temperatures. Environ Sci Technol 42(14):5137–5143. https://doi.org/10.1021/es8002684

Chen X, Zhang NQ, Sun KN (2012) Facile ammonia-induced fabrication of nanoporous NiO films with enhanced lithium-storage properties. Electrochem Commun 20:137–140. https://doi.org/10.1016/j.elecom.2012.04.009

Chen Q, Zheng JW, Wen LY, Yang C, Zhang LJ (2019) A multifunctional-group modified cellulose for enhanced heavy metal cadmium adsorption: performance and quantum chemical mechanism. Chemosphere 224:509–518. https://doi.org/10.1016/j.chemosphere.2019.02.138

Cheng XK, Kan AT, Tomson MB (2004) Naphthalene adsorption and desorption from Aqueous C-60 fullerene. J Chem Eng Data 49(3):675–683. https://doi.org/10.1021/je030247m

Chowdhury I, Duch MC, Mansukhani ND, Hersam MC, Bouchard D (2013) Colloidal properties and stability of graphene oxide nanomaterials in the aquatic environment. Environ Sci Technol 47(12):6288–6296. https://doi.org/10.1021/es400483k

Das O, Sarmah AK, Bhattacharyya D (2015) Structure-mechanics property relationship of waste derived biochars. Sci Total Environ 538:611–620. https://doi.org/10.1016/j.scitotenv.2015.08.073

Dong HR, Ahmad K, Zeng GM, Li ZW, Chen GQ, He Q, Xie YK, Wu YA, Zhao F, Zeng YL (2016) Influence of fulvic acid on the colloidal stability and reactivity of nanoscale zero-valent iron. Environ Pollut 211:363–369. https://doi.org/10.1016/j.envpol.2016.01.017

Hameed R, Lei C, Lin DH (2020) Adsorption of organic contaminants on biochar colloids: effects of pyrolysis temperature and particle size. Environ Sci Pollut Res Int 27(15):18412–18422. https://doi.org/10.1007/s11356-020-08291-5

Hu M, Wu WH, Lin DH, Yang K (2022) Adsorption of fulvic acid on mesopore-rich activated carbon with high surface area. Sci Total Environ 838:155918. https://doi.org/10.1016/j.scitotenv.2022.155918

Huang WL, Yu H, Weber WJ (1998) Hysteresis in the sorption and desorption of hydrophobic organic contaminants by soils and sediments – 1. A comparative analysis of experimental protocols. J Contam Hydrol 31(1–2):129–148. https://doi.org/10.1016/S0169-7722(97)00056-9

Islam MA, Morton DW, Johnson BB, Angove MJ (2020) Adsorption of humic and fulvic acids onto a range of adsorbents in aqueous systems, and their effect on the adsorption of other species: a review. Sep Purif Technol 247:116949. https://doi.org/10.1016/j.seppur.2020.116949

Jellali S, Khiari B, Usman M, Hamdi H, Charabi Y, Jeguirim M (2021) Sludge-derived biochars: a review on the influence of synthesis conditions on pollutants removal efficiency from wastewaters. Renew Sust Energ Rev 144:111068. https://doi.org/10.1016/j.rser.2021.111068

Ji LL, Liu FL, Xu ZY, Zheng SR, Zhu DQ (2009) Zeolite-templated microporous carbon as a superior adsorbent for removal of mono-aromatic compounds from aqueous solution. Environ Sci Technol 43(20):7870–7876. https://doi.org/10.1021/es901497w

Jing FQ, Pan MJ, Chen JW (2018) Kinetic and isothermal adsorption-desorption of PAEs on biochars: effect of biomass feedstock, pyrolysis temperature, and mechanism implication of desorption hysteresis. Environ Sci Pollut Res Int 25(12):11493–11504. https://doi.org/10.1007/s11356-018-1356-0

Kang S, Kim G, Choe JK, Choi Y (2019) Effect of using powdered biochar and surfactant on desorption and biodegradability of phenanthrene sorbed to biochar. J Hazard Mater 371:253–260. https://doi.org/10.1016/j.jhazmat.2019.02.104

Kim HB, Kim SH, Jeon EK, Kim DH, Tsang DCW, Alessi DS, Kwon EE, Baek K (2018) Effect of dissolved organic carbon from sludge, rice straw and spent coffee ground biochar on the mobility of arsenic in soil. Sci Total Environ 636:1241–1248. https://doi.org/10.1016/j.scitotenv.2018.04.406

Koelmans AA, Meulman B, Meijer T, Jonker MT (2009) Attenuation of polychlorinated biphenyl sorption to charcoal by humic acids. Environ Sci Technol 43(3):736–742. https://doi.org/10.1021/es802862b

Lattao C, Cao XY, Mao JD, Schmidt-Rohr K, Pignatello JJ (2014) Influence of molecular structure and adsorbent properties on sorption of organic compounds to a temperature series of wood chars. Environ Sci Technol 48(9):4790–4798. https://doi.org/10.1021/es405096q

Lehmann J, Cowie A, Masiello CA, Kammann C, Woolf D, Amonette JE, Cayuela ML, Camps-Arbestain M, Whitman T (2021) Biochar in climate change mitigation. Nat Geosci 14(12):883–892. https://doi.org/10.1038/s41561-021-00852-8

Lian F, Xing BS (2017) Black carbon (biochar) in water/soil environments: molecular structure, sorption, stability, and potential risk. Environ Sci Technol 51(23):13517–13532. https://doi.org/10.1021/acs.est.7b02528

Lin DH, Pan B, Zhu LZ, Xing BS (2007) Characterization and phenanthrene sorption of tea leaf powders. J Agric Food Chem 55(14):5718–5724. https://doi.org/10.1021/jf0707031

Ma SQ, Jing F, Sohi SP, Chen JW (2019) New insights into contrasting mechanisms for PAE adsorption on millimeter, micron- and nano-scale biochar. Environ Sci Pollut Res Int 26(18):18636–18650. https://doi.org/10.1007/s11356-019-05181-3

Mao SD, Liu SR, Zhou YT, An Q, Zhou XJ, Mao ZY, Wu YT, Liu WP (2021) The occurrence and sources of polychlorinated biphenyls (PCBs) in agricultural soils across China with an emphasis on unintentionally produced PCBs. Environ Pollut 271:116171. https://doi.org/10.1016/j.envpol.2020.116171

Oleszczuk P, Pan B, Xing BS (2009) Adsorption and desorption of oxytetracycline and carbamazepine by multiwalled carbon nanotubes. Environ Sci Technol 43(24):9167–9173. https://doi.org/10.1021/es901928q

Patra BR, Mukherjee A, Nanda S, Dalai AK (2021) Biochar production, activation and adsorptive applications: a review. Environ Chem Lett 19(3):2237–2259. https://doi.org/10.1007/s10311-020-01165-9

Tang L, Yu JF, Pang Y, Zeng GM, Deng YC, Wang JJ, Ren XY, Ye SJ, Peng B, Feng HP (2018) Sustainable efficient adsorbent: alkali-acid modified magnetic biochar derived from sewage sludge for aqueous organic contaminant removal. Chem Eng J 336:160–169. https://doi.org/10.1016/j.cej.2017.11.048

Tong YR, McNamara PJ, Mayer BK (2019) Adsorption of organic micropollutants onto biochar: a review of relevant kinetics, mechanisms and equilibrium. Environ Sci-Wat Res 5(5):821–838. https://doi.org/10.1039/c8ew00938d

Wang DJ, Zhang W, Hao XZ, Zhou DM (2013) Transport of biochar particles in saturated granular media: effects of pyrolysis temperature and particle size. Environ Sci Technol 47(2):821–828. https://doi.org/10.1021/es303794d

Wang F, Ren XH, Sun HW, Ma L, Zhu HK, Xu JY (2016a) Sorption of polychlorinated biphenyls onto biochars derived from corn straw and the effect of propranolol. Bioresour Technol 219:458–465. https://doi.org/10.1016/j.biortech.2016.08.006

Wang ZY, Han LF, Sun K, Jin J, Ro KS, Libra JA, Liu XT, Xing BS (2016b) Sorption of four hydrophobic organic contaminants by biochars derived from maize straw, wood dust and swine manure at different pyrolytic temperatures. Chemosphere 144:285–291. https://doi.org/10.1016/j.chemosphere.2015.08.042

Wang BY, Zhang W, Li H, Fu HY, Qu XL, Zhu DQ (2017a) Micropore clogging by leachable pyrogenic organic carbon: a new perspective on sorption irreversibility and kinetics of hydrophobic organic contaminants to black carbon. Environ Pollut 220:1349–1358. https://doi.org/10.1016/j.envpol.2016.10.100

Wang F, Sun HW, Ren XH, Zhang K (2017b) Sorption of naphthalene and its hydroxyl substitutes onto biochars in single-solute and bi-solute systems with propranolol as the co-solute. Chem Eng J 326:281–291. https://doi.org/10.1016/j.cej.2017.05.159

Wang YL, Lei C, Lin DH (2021) Environmental behaviors and biological effects of engineered nanomaterials: important roles of interfacial interactions and dissolved organic matter. Chin J of Chem 39(2):232–242. https://doi.org/10.1002/cjoc.202000466

Wu T, Liao XY, Zou YT, Liu YZ, Yang K, White JC, Lin DH (2022) Fe-based nanomaterial transformation to amorphous Fe: enhanced alfalfa rhizoremediation of PCBs-contaminated soil. J Hazard Mater 425:127973. https://doi.org/10.1016/j.jhazmat.2021.127973

Xie MX, Chen W, Xu ZY, Zheng SR, Zhu DQ (2014) Adsorption of sulfonamides to demineralized pine wood biochars prepared under different thermochemical conditions. Environ Pollut 186:187–194. https://doi.org/10.1016/j.envpol.2013.11.022

Xu FC, Wei CH, Zeng QQ, Li XN, Alvarez PJJ, Li QL, Qu XL, Zhu DQ (2017) Aggregation behavior of dissolved black carbon: implications for vertical mass flux and fractionation in aquatic systems. Environ Sci Technol 51(23):13723–13732. https://doi.org/10.1021/acs.est.7b04232

Yang F, Gao Y, Sun L, Zhang SS, Li JJ, Zhang Y (2018a) Effective sorption of atrazine by biochar colloids and residues derived from different pyrolysis temperatures. Environ Sci Pollut Res Int 25(19):18528–18539. https://doi.org/10.1007/s11356-018-2077-0

Yang K, Jiang Y, Yang JJ, Lin DH (2018b) Correlations and adsorption mechanisms of aromatic compounds on biochars produced from various biomass at 700 degrees C. Environ Pollut 233:64–70. https://doi.org/10.1016/j.envpol.2017.10.035

Yang W, Shang JY, Li BG, Flury M (2019a) Surface and colloid properties of biochar and implications for transport in porous media. Crit Rev Environ Sci Technol 50(23):2484–2522. https://doi.org/10.1080/10643389.2019.1699381

Yang W, Shang JY, Sharma P, Li BG, Liu KS, Flury M (2019b) Colloidal stability and aggregation kinetics of biochar colloids: effects of pyrolysis temperature, cation type, and humic acid concentrations. Sci Total Environ 658:1306–1315. https://doi.org/10.1016/j.scitotenv.2018.12.269

Yang W, Feng TT, Flury M, Li BG, Shang JY (2020) Effect of sulfamethazine on surface characteristics of biochar colloids and its implications for transport in porous media. Environ Pollut 256:113482. https://doi.org/10.1016/j.envpol.2019.113482

Zhang W, Niu JZ, Morales VL, Chen XC, Hay AG, Lehmann J, Steenhuis TS (2010) Transport and retention of biochar particles in porous media: effect of pH, ionic strength, and particle size. Ecohydrology 3(4):497–508. https://doi.org/10.1002/eco.160

Zhang QR, Wang JM, Lyu H, Zhao Q, Jiang LS, Liu L (2019) Ball-milled biochar for galaxolide removal: sorption performance and governing mechanisms. Sci Total Environ 659:1537–1545. https://doi.org/10.1016/j.scitotenv.2019.01.005

Zhi Y, Liu JX (2018) Sorption and desorption of anionic, cationic and zwitterionic polyfluoroalkyl substances by soil organic matter and pyrogenic carbonaceous materials. Chem Eng J 346:682–691. https://doi.org/10.1016/j.cej.2018.04.042

Zhou FS, Wang H, Fang S, Zhang WH, Qiu RL (2015) Pb(II), Cr(VI) and atrazine sorption behavior on sludge-derived biochar: role of humic acids. Environ Sci Pollut Res Int 22(20):16031–16039. https://doi.org/10.1007/s11356-015-4818-7

Zhou YM, Miao DJ, Gomez-Eyles JL, Ghosh U, Bi MY, Li J, Ren FM (2022) Comparative study on polychlorinated biphenyl sorption to activated carbon and biochar and the influence of natural organic matter. Chemosphere 287:132239. https://doi.org/10.1016/j.chemosphere.2021.132239

Zhu MH, Yuan YB, Yin H, Guo ZY, Wei XP, Qi X, Liu H, Dang Z (2022) Environmental contamination and human exposure of polychlorinated biphenyls (PCBs) in China: a review. Sci Total Environ 805:150270. https://doi.org/10.1016/j.scitotenv.2021.150270